Mortality can produce limit cycles in density-dependent models with a predator-prey relationship

Tahani Mtar, Radhouane Fekih-Salem, Tewfik Sari

MORTALITY CAN PRODUCE LIMIT CYCLES IN DENSITY-DEPENDENT MODELS WITH A PREDATOR-PREY RELATIONSHIP

Tahani Mtar[a] and Radhouane Fekih-Salem[a,c,*] and Tewfik Sari[b]

[a]University of Tunis El Manar, National Engineering School of Tunis, LAMSIN, 1002, Tunis, Tunisia
[b] ITAP, Univ Montpellier, INRAE, Institut Agro, Montpellier, France
[c] University of Monastir, Higher Institute of Computer Science of Mahdia, 5111, Mahdia, Tunisia

Abstract. We study an interspecific, density-dependent model of two species competing for a single nutrient in a chemostat, allowing for a predator-prey relationship between them. We have previously examined the system in the absence of species mortality, showing that multiple positive steady states can appear and disappear through a saddle-node or transcritical bifurcation. In this paper we include mortality. We give a complete analysis for the existence and local stability of all steady states of the three-dimensional system that cannot be reduced to two dimensional ones. Specializing the forms of the rate functions, we show how mortality destabilizes the positive steady state and that stable limit cycles emerge through supercritical Hopf bifurcations. To describe how the process behaves with respect to the choice of dilution rate and input concentration as control parameters, we determine the operating diagram numerically by using the software package MATCONT. The bifurcation diagram based on the input concentration shows various types of bifurcations of steady states, and coexistence either at a positive steady state or via sustained oscillations.

1. **Introduction.** The chemostat is an important laboratory apparatus used for continuous cultures of microorganisms in microbiology and ecology. The mathematical analysis of the classical chemostat model of two or more microbial species competing for a single limiting nutrient shows that only the species with the lowest 'break-even' concentration survives while all other species become extinct (see, for instance, [24, 49]). This result, known as the Competitive Exclusion Principle (CEP), has a long history in the literature of bio-mathematics and in [41] a new proof of this principle is given using elementary analysis and comparisons of solutions of ordinary differential equations.

Although the CEP has been confirmed by the experiments of Hansen and Hubbell [23], this principle is not compatible with the great biodiversity found in nature. Several suggestions to address the disparity in predictions of models involving multiple microbial species with observations from the laboratory can be found in the

2010 *Mathematics Subject Classification.* Primary: 34A34, 34D20; Secondary: 92B05, 92D25.
Key words and phrases. Density-dependence; Hopf Bifurcation; limit cycle; mortality; operating diagram; predator-prey relationship.
Supported by the UNESCO ICIREWARD project ANUMAB and the Euro-Mediterranean research network TREASURE (http://www.inrae.fr/treasure).
* Corresponding author: Radhouane Fekih-Salem.

literature. Note these various mechanisms to promote coexistence: the intraspecific and interspecific competition [1, 10], the flocculation [16, 18, 19, 20, 21], the density-dependence of the growth functions [7, 17, 25, 30, 31, 32, 33, 36], the predator-prey interactions [6, 29], the complex food webs [2, 26, 55], the presence of inhibitors that affects the strongest competitor [3, 11, 12], the commensalistic relationship [4, 5, 45], and the syntrophic relationship [9, 15, 43, 56].

An extension of the classical chemostat model was considered in a series of papers by Lobry et al. [25, 30, 31, 32, 33], taking into account general intraspecific and interspecific density-dependent growth rates with distinct removal rates for each species. Considering particular density-dependent growth functions with intraspecific interference, the numerical simulations in [30] show the coexistence of several species for small enough interspecific interference and the exclusion of one species, at least, for large enough interspecific interference. In [17], a mathematical analysis confirms these numerical results where this system presents the global stability of the coexistence steady state for small enough interspecific interference terms while this system exhibits bi-stability for large enough interspecific interference. With the same removal rates and only interspecific interferences, the coexistence of two species is impossible which consistent with the CEP [14].

The present paper considers a model of two competitors for a single resource in a chemostat, with interspecific density-dependent growth functions. The species have a predator-prey relationship, that is, the first species (the prey) promotes the growth of the second species (the predator) which in turn inhibits the growth of the first species. In our study, the mortality (or decay) of two species is taken into account and not neglected as in previous studies [14, 36].

At time t, let $S(t)$ denote the substrate concentration, and $x_1(t)$ and $x_2(t)$ the concentrations of prey and predator species, respectively. The model can be written as follows:

$$\left\{\begin{array}{lcl} \dot{S} & = & D(S_{in}-S)-f_1(S,x_2)x_1-f_2(S,x_1)x_2, \\ \dot{x}_1 & = & (f_1(S,x_2)-D_1)x_1, \\ \dot{x}_2 & = & (f_2(S,x_1)-D_2)x_2, \end{array}\right. \tag{1}$$

where D and S_{in} represent, respectively, the dilution rate and the input substrate concentration in the chemostat. f_1 is the density-dependent growth rate of the prey species x_1 and it assumed to be increasing in the variable S and decreasing in the predator species x_2. f_2 is the density-dependent growth rate of the predator species x_2 and it assumed to be increasing in the variable S and increasing in the prey species x_1. The removal rate D_i of species x_i can be modeled as in [19, 47] by

$$D_i=\alpha_i D+a_i, \quad i=1,2.$$

where the coefficient α_i belongs to $[0,1]$ and represents the fraction of the prey and predator species leaving the reactor. In [5], this coefficient can model a biomass reactor attached to the support or to decouple the residence time of solids and the hydraulic residence time $(1/D)$. Moreover, a_i is the nonnegative mortality (or decay) rate of the species x_i.

In [14, 36], the mathematical analysis of model (1) shows that the system may exhibit the coexistence or the bi-stability with a multiplicity of positive steady states, in the particular case $\alpha_i=1$ and $a_i=0$. Moreover, in [36], the operating diagram shows that all steady states can appear or disappear only through saddle-node or transcritical bifurcations according to the control parameters represented by the dilution rate, D, and the input concentration, S_{in}, of the substrate. Indeed,

the operating diagram is a very useful tool to determine how a process behaves when all biological parameters are fixed and the control parameters are varied, as they are the most easily manipulated parameters in a chemostat. This diagram is very important to understand the model from the mathematical and biological point of view. It is often built in the mathematical literature (see [1, 3, 8, 9, 11, 12, 17, 20, 24, 36, 42, 43, 44, 54]) and the biological literature (see [27, 45, 52, 56]). In [37], we have studied the existence and the local stability of model (1) in the particular case where $\alpha_i = 1$.

The aim of this paper is to understand the joint effect of mortality and predator-prey relationship on the behavior of the density-dependent model considered in [14, 36]. Our study provides an extension of the results in [14, 36] by considering distinct removal rates where the system cannot be reduced to a two-dimensional one. Using the Routh–Hurwitz criterion, we determine conditions of the existence and local stability of all steady states according to operating parameters D and S_{in}. In contrast to the case without mortality, where the coexistence may occur only around a positive steady state [14, 36], our results show that the mortality can destabilize the positive steady state through Hopf bifurcation where the coexistence can be around a stable limit cycle. It is known that introducing decay for the species in the classical predator-prey models in the chemostat results in instability and chaos [28]. For more details on food-chains in the chemostat, the reader may consult [6, 50, 51]. In our model, the same intrinsic effect of mortality on the stability of the positive steady state is observed. Indeed, when mortality is included in the density-dependent model with predator-prey relationship, the positive steady state is not necessarily stable, when it exists. On the other hand, our study provides an important tool which is the operating diagram to determine the region of the emergence of stable limit cycles theoretically from Routh–Hurwitz conditions and numerically by using the software MATCONT [35]. Finally, according to the control parameter S_{in} a one-parameter bifurcation diagram determines all types of bifurcations.

The paper is structured as follows. We first introduce in Section 2 assumptions on the growth functions and preliminary results. Then we determine the necessary and sufficient conditions of existence and stability of the steady states using the nullcline method. In Section 3, we determine theoretically the operating diagrams and then numerically by using MATCONT. Section 4 deals, with respect to the input concentration S_{in}, the one-parameter bifurcation diagram and the Hopf bifurcation. The numerical simulations validate the theoretical analysis of the operating diagram. Some conclusions are drawn in Section 5. Finally, all the parameter values used in simulations are provided in Appendix A and the definitions of the various auxiliary functions used in our paper are summarized in Appendix B.

2. **Assumptions and mathematical analysis.**

In this paper, we assume that the growth functions $f_1(S, x_2)$ and $f_2(S, x_1)$ are continuously differentiable ($\mathcal{C}^1$) and satisfy the following hypotheses.

(H1) For all $x_j \geqslant 0$ and $S > 0$, $f_i(0, x_j) = 0$ and $f_2(S, 0) = 0$.

(H2) For all $S > 0$, $x_1 > 0$ and $x_2 \geqslant 0$, $\frac{\partial f_i}{\partial S}(S, x_j) > 0$, $\frac{\partial f_1}{\partial x_2}(S, x_2) < 0$ and $\frac{\partial f_2}{\partial x_1}(S, x_1) > 0$.

Assumption (H1) means that the substrate is necessary for the growth of each species and the prey species x_1 is necessary for the growth of the predator species

x_2. Assumption (H2) means that the growth rate of the prey species x_1 increases with the concentration of the substrate S and is inhibited by the predator species x_2, whereas the growth of the predator species x_2 increases with both the concentrations of S and the prey species x_1. We now prove the following result.

Proposition 1. *Assume that assumptions (H1)-(H2) hold. For any nonnegative initial condition, the solution of system (1) exists for all $t \geqslant 0$, remains nonnegative and is bounded. In addition, the set*

$$\Omega = \left\{(S, x_1, x_2) \in \mathbb{R}^3_+ : S + x_1 + x_2 \leqslant DS_{in}/D_{\min}\right\}$$

is positively invariant and is a global attractor for the dynamics (1), where $D_{\min} = \min(D, D_1, D_2)$.

Proof. Since the vector field defined by (1) is C^1, the uniqueness of the solution to an initial value problem holds. The boundary faces defined by $x_1 = 0$ and $x_2 = 0$ are invariant under the vector field defined by system (1). Therefore, for any nonnegative initial condition, $x_1(t)$ and $x_2(t)$ are always nonnegative. Assume that $S(0) \geqslant 0$ and that there exists $t_0 > 0$ such that $S(t_0) = 0$ and that $S(t) > 0$ for $t \in (0, t_0)$. Then $\dot{S}(t_0) \leqslant 0$. On the other hand, $S(t_0) = 0$ implies $\dot{S}(t_0) = DS_{in} > 0$, which is a contradiction. Therefore, $S(t)$ is always nonnegative. Let $z = S + x_1 + x_2$. From system (1), we have

$$\dot{z} = D(S_{in} - S) - D_1 x_1 - D_2 x_2.$$

Consequently,

$$\dot{z} \leqslant D_{\min}(DS_{in}/D_{\min} - z).$$

Using Gronwall's lemma, we obtain

$$z(t) \leqslant DS_{in}/D_{\min} + (z(0) - DS_{in}/D_{\min})e^{-D_{\min}t} \quad \text{for all} \quad t \geqslant 0. \tag{2}$$

We deduce that

$$z(t) \leqslant \max\left\{z(0), DS_{in}/D_{\min}\right\} \quad \text{for all} \quad t \geqslant 0.$$

Therefore, the solutions of (1) are positively bounded and are defined for all $t \geqslant 0$. From (2), we deduce that the set Ω is positively invariant and is a global attractor for (1). □

Now we discuss the existence of steady states of system (1). A steady state of (1) exists or is said to be 'meaningful' if and only if all its components are nonnegative. The steady states are given by the solutions of the following system:

$$\begin{cases} 0 &= D(S_{in} - S) - f_1(S, x_2)x_1 - f_2(S, x_1)x_2, \\ 0 &= (f_1(S, x_2) - D_1)x_1, \\ 0 &= (f_2(S, x_1) - D_2)x_2. \end{cases} \tag{3}$$

If $x_1 = 0$ and $x_2 > 0$, we obtain $D_2 = 0$ from assumption (H1), which is impossible. Thus, system (1) can have at most three types of steady states labeled as follows:

- $\mathcal{E}_0$ ($x_1 = x_2 = 0$): the washout of two species which always exists.
- $\mathcal{E}_1$ ($x_1 > 0$, $x_2 = 0$): only prey species is present.
- $\mathcal{E}^*$ ($x_1 > 0$, $x_2 > 0$): the coexistence of two species.

Since the function $S \mapsto f_1(S, 0)$ is increasing (see (H2)), the equation $f_1(S, 0) = D_1$ has a unique solution, for all $D < (f_1(+\infty, 0) - a_1)/\alpha_1$. This solution is noted

$\lambda_1(D)$ and called the *break-even concentration*. If $D \geq (f_1(+\infty, 0) - a_1)/\alpha_1$, we let $\lambda_1(D) = +\infty$. Therefore

$$f_1(S, 0) = D_1 \Longleftrightarrow S = \lambda_1(D). \tag{4}$$

The following result determines the existence condition of the steady state $\mathcal{E}_1$ according to operating parameters.

Proposition 2. *Assume that (H1) and (H2) hold. The boundary steady state* $\mathcal{E}_1 = (\tilde{S}, \tilde{x}_1, 0)$ *of system (1) is defined by*

$$\tilde{S} = \lambda_1(D) \quad \textit{and} \quad \tilde{x}_1 = \tfrac{D}{D_1}(S_{in} - \lambda_1(D)). \tag{5}$$

It exists if and only if

$$S_{in} > \lambda_1(D). \tag{6}$$

When it exists, $\mathcal{E}_1$ *is unique.*

Proof. For $\mathcal{E}_1$, $x_1 > 0$ and $x_2 = 0$. From the second equation of (3) and the definition (4) of the break-even concentration, it follows that $S = \lambda_1(D)$. From the first equation of (3), we obtain the x_1 component. Thus, $\mathcal{E}_1$ exists if and only if $x_1 > 0$, that is, condition (6) holds. □

Next we determine existence conditions for positive steady states $\mathcal{E}^* = (S^*, x_1^*, x_2^*)$ where $S^* > 0$, $x_1^* > 0$, and $x_2^* > 0$. Thus, positive steady states are solutions to this set of equations equivalent to (3)

$$\begin{aligned} D(S_{in} - S) &= D_1 x_1 + D_2 x_2 & (7)\\ f_1(S, x_2) &= D_1 & (8)\\ f_2(S, x_1) &= D_2. & (9) \end{aligned}$$

From (7), the solution S^* is given by

$$S^* = S_{in} - D_1 x_1^*/D - D_2 x_2^*/D. \tag{10}$$

Replacing S^* by this expression in (8,9), we see that $(x_1 = x_1^*, x_2 = x_2^*)$ must be a solution of

$$\begin{cases} \widetilde{f}_1(x_1, x_2) := f_1(S_{in} - D_1 x_1/D - D_2 x_2/D, x_2) - D_1 = 0 \\ \widetilde{f}_2(x_1, x_2) := f_2(S_{in} - D_1 x_1/D - D_2 x_2/D, x_1) - D_2 = 0. \end{cases} \tag{11}$$

Note that the functions $\widetilde{f}_1$ and $\widetilde{f}_2$ are defined on the set

$$M := \left\{(x_1, x_2) \in \mathbb{R}_+^2 : D_1 x_1/D + D_2 x_2/D \leqslant S_{in}\right\}.$$

In addition, S^* is positive if and only if $D_1 x_1^*/D + D_2 x_2^*/D < S_{in}$, that is, (11) has a positive solution in the interior $\mathring{M}$ of M. In what follows, we define the line δ by $D_1 x_1/D + D_2 x_2/D = S_{in}$ and we need the next notations:

$$E = \tfrac{\partial f_1}{\partial S}, \quad F = \tfrac{\partial f_2}{\partial S}, \quad G = -\tfrac{\partial f_1}{\partial x_2}, \quad H = \tfrac{\partial f_2}{\partial x_1}. \tag{12}$$

We have used the opposite sign of the partial derivative $G = -\partial f_1/\partial x_2$, such that all quantities involved in the following computations are positive. To solve (11) in $\mathring{M}$, we need the following Lemmas 1, 2 and 3 where the proofs of Lemmas 1 and 3 are similar to those in [37].

Lemma 1. *Make assumptions (H1) and (H2), assume that $S_{\text{in}} > \lambda_1(D)$, so that a unique boundary steady state $\mathcal{E}_1 = (\tilde{S}, \tilde{x}_1, 0)$ exists according to Proposition 2. The equation $\widetilde{f}_1(x_1, x_2) = 0$ defines a smooth decreasing function*

$$\begin{array}{rccc} F_1 & : & [0, \tilde{x}_1] & \longrightarrow & [0, \tilde{x}_2] \\ & & x_1 & \longmapsto & F_1(x_1) = x_2, \end{array}$$

such that $F_1(\tilde{x}_1) = 0$, $F_1(0) = \tilde{x}_2$ and

$$-\tfrac{D_1}{D_2} < F_1'(x_1) = -\tfrac{D_1 E}{D_2 E + DG} < 0, \quad \text{for all} \quad x_1 \in [0, \tilde{x}_1], \tag{13}$$

where $\tilde{x}_2$ is the unique solution of the equation $\widetilde{f}_1(0, x_2) = 0$. In addition, the graph γ_1 of F_1 lies in $\mathring{M}$, that is, $(x_1, F_1(x_1)) \in \mathring{M}$ for all $x_1 \in (0, \tilde{x}_1)$ (see Fig. 2).

To define the function $x_2 = F_2(x_1)$ of equation $\widetilde{f}_2(x_1, x_2) = 0$, we will need the following Lemma to determine the necessary and sufficient condition for the existence of solutions of the equation $\widetilde{f}_2(x_1, 0) = 0$.

Lemma 2. *Under assumptions (H1)-(H2), the equation $\widetilde{f}_2(x_1, 0) = 0$ has a solution in $[0, DS_{in}/D_1]$ if and only if,*

$$\max_{x_1 \in [0, DS_{in}/D_1]} f_2(S_{in} - D_1 x_1/D, x_1) \geqslant D_2. \tag{14}$$

Generically, we have an even number of solutions in $[0, DS_{in}/D_1]$.

Proof. Under assumptions (H1)-(H2), the function $x_1 \longmapsto \widetilde{f}_2(x_1, 0)$ is continuous on $[0, DS_{in}/D_1]$ with $\widetilde{f}_2(0, 0) = \widetilde{f}_2(DS_{in}/D_1, 0) = -D_2$. Consequently, the equation $\widetilde{f}_2(x_1, 0) = 0$ has a solution in $[0, DS_{in}/D_1]$ if and only if

$$\max_{x_1 \in [0, DS_{in}/D_1]} \widetilde{f}_2(x_1, 0) \geqslant 0$$

that is, condition (14) holds (see Fig. 1). □

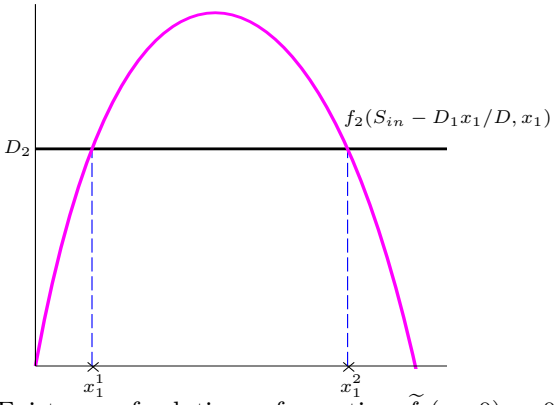

FIGURE 1. Existence of solutions of equation $\widetilde{f}_2(x_1, 0) = 0$. The color in this figure and all other Figures is available online only.

For simplicity, we add the following assumption which is satisfied by the specific growth rates (31).

(H3) Equation $\widetilde{f}_2(x_1, 0) = 0$ has at most two solutions x_1^1 and x_1^2 in $[0, DS_{in}/D_1]$.

The proof of the maximum number of solutions of the equation $\widetilde{f}_2(x_1, 0) = 0$ for

the specific growth rates (31) is similar to that in Appendix B of [37]. When the function $x_1 \longmapsto \widetilde{f}_2(x_1, 0)$ is multimodal, the study of this general case can be treated similarly, without added difficulty. In this particular case, we obtain the next result.

Lemma 3. *Assume that assumptions (H1) to (H3) and condition (14) hold. Then, the equation $\widetilde{f}_2(x_1, x_2) = 0$ defines a smooth function*

$$\begin{array}{rccc} F_2 & : & [x_1^1, x_1^2] & \longrightarrow & [0, DS_{in}/D_2) \\ & & x_1 & \longmapsto & F_2(x_1) = x_2, \end{array}$$

such that $F_2(x_1^1) = F_2(x_1^2) = 0$ and

$$-\tfrac{D_1}{D_2} < F_2'(x_1) = -\tfrac{D_1}{D_2} + \tfrac{D}{D_2}\tfrac{H}{F}, \quad \text{for all} \quad x_1 \in [x_1^1, x_1^2], \tag{15}$$

where x_1^1 and x_1^2 are the solutions of the equation $\widetilde{f}_2(x_1, 0) = 0$. In addition, the graph γ_2 of F_2 lies in $\mathring{M}$ where $(x_1, F_2(x_1)) \in \mathring{M}$ for all $x_1 \in (x_1^1, x_1^2)$ (see Fig. 2).

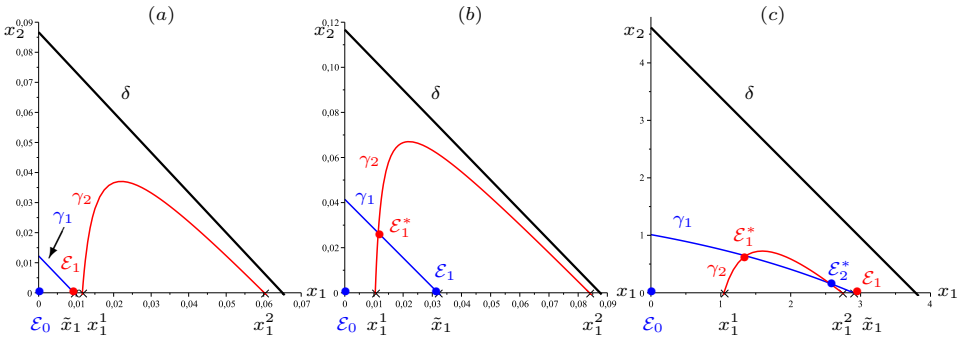

FIGURE 2. Number of positive steady states: (a) Case 1: no positive steady state when $(S_{in}, D) = (0.26, 0.1)$, (b) Case 2: an odd number when $(S_{in}, D) = (0.35, 0.1)$, (c) Case 3: an even number when $(S_{in}, D) = (4.5, 0.8)$.

Using Lemmas 1, 2, and 3, we can give necessary and sufficient conditions for the existence of coexistence steady states $\mathcal{E}^*$.

Proposition 3. *Coexistence steady states $\mathcal{E}^*$ of (1) exist if and only if the curves γ_1 and γ_2 intersect in $\mathring{M}$. In this case x_1^* and x_2^* are positive solutions to the equations*

$$x_2 = F_1(x_1) \quad \text{and} \quad x_2 = F_2(x_1). \tag{16}$$

and S^* is given by (10).

Proof. From (11) and Lemmas 1 and 3, a coexistence steady state exists if and only if the curves γ_1 and γ_2 have a positive intersection, that is, (x_1^*, x_2^*) is a solution of (16). If the intersection exists, then we have

$$D_1 x_1^*/D + D_2 x_2^*/D < S_{\text{in}}.$$

Consequently, the component S^* which defined by (10), is positive. □

According to the position of $\tilde{x}_1$ relative to x_1^1 and x_1^2, we distinguish three cases:

$$\text{Case 1}: \ \tilde{x}_1 < x_1^1 < x_1^2, \quad \text{Case 2}: \ x_1^1 < \tilde{x}_1 < x_1^2, \quad \text{Case 3}: \ x_1^1 < x_1^2 < \tilde{x}_1. \tag{17}$$

In the first case, the graphs of F_1 and F_2 have disjoint domains (see Fig. 2). By the definitions of these functions, $\widetilde{f}_1(x_1, x_2) = 0$ and $\widetilde{f}_2(x_1, x_2) = 0$ have no point in common. In the second case, the domains overlap. The conditions $F_1(\tilde{x}_1) = 0$ and

$F_2(x_1^1) = 0$ imply that the loci must cross at least once. In the third case, the domain of F_2 is completely contained within the domain F_1. If the graph of F_2 is completely below the graph of F_1, there is again no point common to both loci. On the other hand, if the graph of F_2 rises above the graph of F_1, then $F_2(x_1^1) = 0 = F_2(x_1^2)$ implies at least two crossings of the loci. The following proposition determines the existence and multiplicity of positive steady states of (1).

Proposition 4. *Assume that hypotheses (H1) to (H3) and conditions (6) and (14) hold.*

1. *In Case 1, there is no positive steady state.*
2. *In Case 2, there exists at least one positive steady state. Generically, the system has an odd number of positive steady states.*
3. *In Case 3, generically system (1) has no positive steady state or an even number of positive steady states.*

According to the three cases given above, one can state the following lemma.

Lemma 4. *Under hypotheses (H1)-(H3) and condition (14), one has*

$$f_2\left(\lambda_1(D), \tfrac{D}{D_1}(S_{in} - \lambda_1(D))\right) < D_2 \;\Leftrightarrow\; \textit{Case 1 or Case 3} \tag{18}$$

$$f_2\left(\lambda_1(D), \tfrac{D}{D_1}(S_{in} - \lambda_1(D))\right) > D_2 \;\Leftrightarrow\; \textit{Case 2.} \tag{19}$$

Proof. Using expression (5) of $\tilde{x}_1$, if Case 1 of (17) holds, that is, if $\tilde{x}_1 < x_1^1$ we have (see Fig. 1)

$$\widetilde{f}_2(\tilde{x}_1, 0) < \widetilde{f}_2(x_1^1, 0)$$

then

$$f_2\left(\lambda_1(D), \tfrac{D}{D_1}(S_{in} - \lambda_1(D))\right) < D_2.$$

In the same way, if Case 3 of (17) holds, that is, if $x_1^2 < \tilde{x}_1$ one has (see Fig. 1)

$$\widetilde{f}_2(\tilde{x}_1, 0) < \widetilde{f}_2(x_1^2, 0)$$

and we reach the same conclusion.
On the other hand, if Case 2 of (17) holds, that is, if $x_1^1 < \tilde{x}_1 < x_1^2$ we obtain (see Fig. 1)

$$\widetilde{f}_2(x_1^1, 0) < \widetilde{f}_2(\tilde{x}_1, 0)$$

which reduces to

$$D_2 < f_2\left(\lambda_1(D), \tfrac{D}{D_1}(S_{in} - \lambda_1(D))\right)$$

It is clear to show the other sense of the two equivalences. □

Now, we determine the local stability of all steady states of (1), using the abbreviation LES for locally exponentially stable steady states.

Proposition 5. *Assume that assumptions (H1)-(H3) hold.*

1. *$\mathcal{E}_0$ is LES if and only if $S_{in} < \lambda_1(D)$.*
2. *$\mathcal{E}_1$ is LES if and only if (18) holds.*
3. *$\mathcal{E}^* = (S^*, x_1^*, x_2^*)$ is LES if and only if $F_1'(x_1^*) < F_2'(x_1^*)$ and*

$$\begin{aligned} c_4(S_{in}, D) := {} & D_1E^2x_1^2 + D_2F^2x_2^2 + DD_1Ex_1 + DD_2Fx_2 \\ & + (D_1EF + (D_1 - D)FG + D_2EF + (D - D_2)EH)x_1x_2 \\ & + (EH - FG + GH)(Ex_1^2x_2 + Fx_1x_2^2) > 0 \end{aligned} \tag{20}$$

where the functions E, F, G are H are defined by (12), and are evaluated at $\mathcal{E}^*$.

Proof. Using the notation (12), the Jacobian matrix of (1) at (S, x_1, x_2) corresponds to the 3×3 matrix:

$$J = \begin{bmatrix} -D - Ex_1 - x_2F & -f_1(S, x_2) - Hx_2 & Gx_1 - f_2(S, x_1) \\ Ex_1 & f_1(S, x_2) - D_1 & -Gx_1 \\ Fx_2 & Hx_2 & f_2(S, x_1) - D_2 \end{bmatrix}.$$

For $\mathcal{E}_0 = (S_{in}, 0, 0)$, the eigenvalues are the roots of the following characteristic polynomial

$$P(\lambda) = (\lambda + D)(\lambda + D_2)(f_1(S_{in}, 0) - D_1 - \lambda).$$

Thus, $\mathcal{E}_0$ is LES if and only if $f_1(S_{in}, 0) < D_1$, that is, $S_{in} < \lambda_1(D)$.

For $\mathcal{E}_1 = (\lambda_1(D), \tilde{x}_1, 0)$, the characteristic polynomial is

$$P(\lambda) = \left(\widetilde{f}_2(\tilde{x}_1, 0) - \lambda\right)(\lambda^2 + c_1\lambda + c_2),$$

where $c_1 = D + \tilde{x}_1 E$ and $c_2 = D_1\tilde{x}_1 E$. Since $c_1 > 0$ and $c_2 > 0$, the real parts of the roots of the quadratic factor are negative. Therefore, $\mathcal{E}_1$ is LES if and only if $\widetilde{f}_2(\tilde{x}_1, 0) < 0$, that is, condition (18) holds.

For $\mathcal{E}^* = (S^*, x_1^*, x_2^*)$, the characteristic polynomial is

$$P(\lambda) = \lambda^3 + c_1\lambda^2 + c_2\lambda + c_3, \tag{21}$$

where

$$\begin{aligned} &c_1 = D + Ex_1^* + Fx_2^*, \quad c_2 = D_1Ex_1^* + D_2Fx_2^* + (GH + EH - FG)x_1^*x_2^* \\ &c_3 = (DGH + D_2EH - D_1FG)x_1^*x_2^*. \end{aligned} \tag{22}$$

Since $c_1 > 0$, according to the Routh–Hurwitz criterion, $\mathcal{E}^*$ is LES if and only if

$$c_3 > 0 \quad \text{and} \quad c_4(S_{in}, D) = c_1c_2 - c_3 > 0 \tag{23}$$

where the function c_4 can be written as its expression (20). Using the expressions of F_1' in (13) and of F_2' in (15), we obtain

$$F_1'(x_1) - F_2'(x_1) = \tfrac{D_1FG - D_2EH - DGH}{D_2F(D_2E/D + G)}.$$

Consequently, at $\mathcal{E}^*$, we have

$$c_3 = \left(F_2'(x_1^*) - F_1'(x_1^*)\right) D_2F[D_2E/D + G]x_1^*x_2^*. \tag{24}$$

Thus, E^* is LES if and only if $F_2'(x_1^*) > F_1'(x_1^*)$ and condition (20) holds. □

Remark 1. In the particular case without mortality of species ($D_i = D$), the Routh–Hurwitz coefficient given by (20) becomes

$$c_4(S_{in}, D) = D(E^2x_1^2 + F^2x_2^2 + D(Ex_1 + Fx_2)) + 2DEFx_1x_2 + \frac{c_3}{D}(Ex_1 + Fx_2),$$

where the expression of c_3 is given by (22). Using the second expression of c_3 given by (24), we find the result of [36] in this particular case $D_i = D$ such that the stability of the coexistence steady state $\mathcal{E}^*$ depends on the sign of $F_2'(x_1^*) - F_1'(x_1^*)$, or, equivalently, the relative directions of the curves γ_1 and γ_2 where they intersect.

3. **Operating diagrams.**

In this section, we will study theoretically and numerically the operating diagram of system (1).

3.1. **Numerical and theoretical methods to determine the operating diagram.** The operating diagrams allows to understand and classify the qualitative changes of the asymptotic behavior of (1) under variation of the operating (or control) parameters which are the concentration of the substrate in the feed bottle S_{in} and the dilution rate D. They have been studied in the existing literature with three different methods.

The first method consists in a numerical exploration of the set of operating parameters D and S_{in}. More precisely, considering a point (D, S_{in}) in this set, the algebraic equations giving the steady states are numerically solved, through the use of Matlab or any other scientific computing platform, and for each meaningful steady state (i.e. with nonnegative components), the characteristic polynomial can be solved, in turn, to determine if the steady state is stable [53]. This method was used in several papers [22, 27, 44, 52, 53, 54]. The advantage of this method is that the determination of the operating diagram does not require a complete mathematical study of the model so that this method can be applied for very complex process including a large number of variables and parameters. However, the accuracy of the results depends on the step used for the discretization of the set of operating parameters. For example, important phenomena were not detected in [52], as the emergence of limit cycles through Hopf bifurcations, which were discovered in the studies using analytical methods [38, 39, 44].

The second method is also numerical and consists in determining the values of critical parameters and different types of bifurcations in systems of autonomous ODEs depending on parameters. Some software is set up, such as MATCONT, CONTENT, AUTO and XPPAUT [13]. This method has the advantage of detecting more complex and subtle bifurcations. It was used in [48] and permitted to detect Bogdanov-Takens and Bautin bifurcations in the model studied in [52].

The third method is theoretical and consists in determining the boundaries of the regions of the diagram, i.e. to compute the parameter values at which a qualitative change in the dynamic behavior of the system occurs. More precisely, the conditions of existence and stability of all steady states must be determined according to the operating parameters. To illustrate the operating diagram, the specific growth rates must be chosen by fixing all the biological parameters. Although the method is called theoretical, the determination of the various curves may require numerical experiments using a scientific numerical platform. The advantages of this method is that in some cases, it can be applied for growth rates which are not specified and must simply verify the general assumptions on the model. Therefore, it is a useful tool to predict the behavior of the system [1, 3, 8, 9, 11, 12, 17, 20, 22, 36, 43].

3.2. **The method of steady-state characteristics.** We use the method of *steady-state characteristics*, introduced by Lobry et al. [32, 33]. This method provides a geometric description of the existence and the asymptotic stability of all steady states, see for instance [1, 17, 19]. It makes it possible to determine the curves where saddle-node bifurcations or Hopf bifurcations occur.

Firstly, let $S \geqslant 0$. From (H2), the function $x_2 \mapsto f_1(S, x_2)$ is decreasing. Thus, the equation $f_1(S, x_2) = D_1$ has a unique solution $x_2 = X_2(S, D)$ if and only if

$$(f_1(S, +\infty) - a_1)/\alpha_1 < D \leqslant (f_1(S, 0) - a_1)/\alpha_1, \text{ that is }, S \in I_1 = [\lambda_1(D), \lambda_1'(D)),$$

where $\lambda_1(D)$ is defined by (4) and $\lambda_1'(D)$ is the unique solution, if it exists, of equation $f_1(S, +\infty) = \alpha_1 D + a_1$. If $D > (f_1(S, +\infty) - a_1)/\alpha_1$ for all $S \geqslant 0$, then

we put $\lambda_1'(D) = +\infty$. Therefore

$$f_1(S, x_2) = D_1 \Longleftrightarrow x_2 = X_2(S, D). \tag{25}$$

Note that the function $S \mapsto X_2(S, D)$ is increasing and satisfies $X_2(\lambda_1(D), D) = 0$ and $X_2(\lambda_1'(D), D) = +\infty$.

On the other hand, the function $x_1 \mapsto f_2(S, x_1)$ is increasing. Thus, the equation $f_2(S, x_1) = D_2$ has a unique solution $x_1 = X_1(S, D)$ if and only if

$$D < (f_2(S, +\infty) - a_2)/\alpha_2, \text{ that is }, S > \lambda_2'(D),$$

where $\lambda_2'(D)$ is the unique solution, if it exists, of equation $f_2(S, +\infty) = \alpha_2 D + a_2$. If $D > (f_2(S, +\infty) - a_2)/\alpha_2$ for all $S \geqslant 0$, then we put $\lambda_2'(D) = +\infty$. Therefore,

$$f_2(S, x_1) = D_2 \Longleftrightarrow x_1 = X_1(S, D). \tag{26}$$

Note that the function $S \mapsto X_1(S, D)$ is decreasing and satisfies $X_1(\lambda_2'(D), D) = +\infty$. Moreover, the function $D \mapsto X_1(S, D)$ is increasing.

We begin by giving equivalent conditions to (18) and (19). We have the following result.

Proposition 6. *Assume that hypotheses (H1)-(H3) and condition (14) hold. Condition (18) is equivalent to*

$$S_{in} < \lambda_1(D) + \tfrac{D_1}{D} X_1(\lambda_1(D), D) = \varphi(D). \tag{27}$$

Inversely, condition (19) is equivalent to $S_{in} > \varphi(D)$.

Proof. Let $S \geqslant 0$. Since the function $D \mapsto X_1(S, D)$ is increasing, the condition (18) is equivalent to

$$\tfrac{D}{D_1}(S_{\text{in}} - \lambda_1(D)) < X_1(\lambda_1(D), D).$$

This completes the proof. □

The necessary and sufficient conditions of existence and local stability of all steady states of (1) according to the operating parameters S_{in} and D are summarized in Table 1.

TABLE 1. Necessary and sufficient conditions of existence and stability of steady states of system (1) where c_4 is defined by (20).

	Existence	Local stability
$\mathcal{E}_0$	always exists	$S_{in} < \lambda_1(D)$
$\mathcal{E}_1$	$S_{in} > \lambda_1(D)$	$S_{in} < \varphi(D)$
$\mathcal{E}^*$	(16) has a solution	$F_2'(x_1^*) > F_1'(x_1^*)$ and $c_4(S_{in}, D) > 0$

From Table 1, $\mathcal{E}_0$ always exists and it is stable in the region bounded by the subset Υ_1 defined in Table 2 and located at the left of this subset (see Fig. 6). $\mathcal{E}_1$ exists in the region located at the right of the subset Υ_1 and it is stable in the region located at the left of the subset Υ_2. The coexistence steady state $\mathcal{E}^*$ exists if and only if (16) has a solution, that is, the curves γ_1 and γ_2 have a positive intersection. In fact, a coexistence steady state emerges or disappears by crossing the subset Υ_2 in the operating plan. But, there can be emergence of two positive steady states via a saddle-node bifurcation when the curve γ_1 of the function $x_1 \mapsto F_1(x_1)$ is tangent to the curve γ_2 of the function $x_1 \mapsto F_2(x_1)$ (see Fig. 2). In this case, similarly to

the analysis of the operating diagram in our paper Mtar et al. [36], the subset in the plan (S_{in}, D) corresponding to a saddle-node bifurcation is defined by

$$\Upsilon_3 := \{(S_{in}, D) : F_1(x_1) = F_2(x_1) \text{ and } F_1'(x_1) = F_2'(x_1)\}, \tag{28}$$

where the solution x_1 depends on S_{in} and D. To determine the subset Υ_4 defined by $c_4(S_{in}, D) = 0$ corresponding to the destabilization of the positive steady state via a Hopf bifurcation, we use the concept of *steady-state characteristics*.

A positive steady state $\mathcal{E}^* = (S^*, x_1^*, x_2^*)$ is a solution of the set of equations

$$\begin{cases} D(S_{in} - S) &= D_1 x_1 + D_2 x_2, \\ f_1(S, x_2) &= D_1, \\ f_2(S, x_1) &= D_2. \end{cases} \tag{29}$$

The second equation of (29) has a unique solution, $x_2 = X_2(S, D)$, and the third equation of (29) has a unique solution, $x_1 = X_1(S, D)$. From the first equations of (29), $S^*(S_{in}, D)$ is the solution of equation

$$D(S_{in} - S) = K(S, D) = D_1 X_1(S, D) + D_2 X_2(S, D). \tag{30}$$

Moreover, the function $K(\cdot, D)$ is defined on $[\max(\lambda_1(D), \lambda_2'(D)), \lambda_1'(D))$ so that the functions $X_1(\cdot, D)$ and $X_2(\cdot, D)$ are positive. It tends to infinity as S tends to $\lambda_1'(D)$ and is non-monotonic (see Fig. 4). Let

$$S_{in}^{\mathrm{SN}}(D) := \tfrac{K(S_{\mathrm{SN}}(D), D)}{D} + S_{\mathrm{SN}}(D),$$

where $S = S_{\mathrm{SN}}(D)$ is the unique solution of equation $\partial K/\partial S = -D$. Thus, we can define differently the subset Υ_3 (28) in Table 2.

Let $C_j(S)$, $j = 3, 4$ be the functions defined by formulas (22) and (23), respectively, where the functions E, F, G and H are defined in (12). Originally, we observed these quantities depend on S, x_1, and x_2, but now we take $x_1 = X_1(S, D)$ and $x_2 = X_2(S, D)$ and view these quantities as functions of S alone. More precisely, we have

$$c_j(S_{in}, D) = C_j(S^*(S_{in}, D)), \quad j = 3, 4,$$

where $S^*(S_{in}, D)$ is a solution of equation (30).

Table 2 summarizes the set $\Upsilon = \{\Upsilon_1, \Upsilon_2, \Upsilon_3, \Upsilon_4\}$ which are the boundaries of different regions of the (S_{in}, D)-plane.

TABLE 2. The set Υ and the corresponding colors in Figs. 6 and 7 where $\varphi(D)$ and c_4 are defined by (27) and (20), resp.

Υ	Color
$\Upsilon_1 = \{(S_{in}, D) : S_{in} = \lambda_1(D)\}$	Black
$\Upsilon_2 = \{(S_{in}, D) : S_{in} = \varphi(D)\}$	Blue
$\Upsilon_3 := \{(S_{in}, D) : S_{in} = S_{in}^{\mathrm{SN}}(D)\}$	
$\Upsilon_4 = \{(S_{in}, D) : c_4(S_{in}, D) = 0\}$	Green

In what follows, due to the impossibility of having an explicit expression for Υ_4, we consider specified growth functions and fixed biological parameter values and we use MAPLE [34] to determine and draw this subset and to verify the condition of stability $F_2'(x_1^*) > F_1'(x_1^*)$ of the steady state $\mathcal{E}^*$. We will also use MATCONT [35] to plot numerically the operating diagram and compare it with the diagram obtained theoretically.

3.3. **Application to specific growth functions.** To construct the operating diagram, the method described in the previous section can be applied to all growth rates satisfying assumptions (H1)-(H3). Let us illustrate this on the following specific growth rates that satisfy the conditions (H1)-(H3):

$$f_1(S,x_2)=\frac{m_1 S}{K_1+S}\frac{1}{1+x_2/L_1},\quad f_2(S,x_1)=\frac{m_2 S}{K_2+S}\frac{x_1}{L_2+x_1}, \tag{31}$$

where m_1, m_2 are the maximum growth rates; K_1, K_2 and L_2 are the Michaelis–Menten constants; L_1 is the inhibition factor due to x_2 for the growth of the species x_1. The values of these biological parameters are given in Table 7.

For the numerical simulations, we have used MAPLE [34] to plot the Figs. 1, 2, 3, 4, 5, 6, 8, and 10, MATCONT [35] for Fig. 7 and Scilab [46] for Figs. 9, 11, 12 and 13. The limit cycles in Figs. 9, 12 and 13 were plotted by solving the ordinary differential equations using the default solver "*lsoda*" from the ODEPACK package in Scilab.

Fig. 3 illustrates that the function $C_3(S)$ is positive for various values of D from the starting points in red of coordinates $(\max(\lambda_1(D),\lambda_2'(D)),0)$. Note that for the specific growth rates (31), $\lambda_1'(D)=+\infty$ since $D_1>f_1(S,+\infty)=0$ for all $S\geqslant 0$. According to (24), the positivity of $C_3(S)$ shows that $F_2'(x_1^*)>F_1'(x_1^*)$ for this set of parameters in Table 7. Thus, Υ_3 is empty and system (1) cannot exhibit a multiplicity of positive steady states appearing through saddle-node bifurcations. In Mtar et al. [36], we have already show how we can determine the subset Υ_3 corresponding to a saddle-node bifurcation. In Fig. 4, the curve of the function

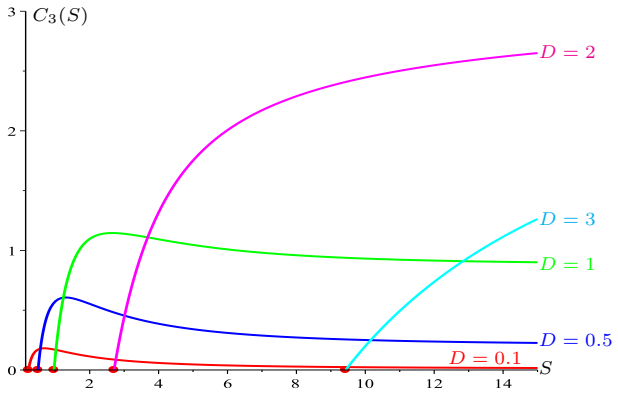

FIGURE 3. Curves of the function $C_3(S)$ for different values of D when $S>\max(\lambda_1(D),\lambda_2'(D))$.

$K(S,D)$ is colored in blue when $C_4(S)<0$, that is, when the positive steady state is unstable. It is colored in red when $C_4(S)>0$, that is, when the positive steady state is stable. From (30), the critical value of S_{in} corresponding to Hopf bifurcation when $C_4(S)=0$ (or also when the curve of $K(S,D)$ changes color) is given by

$$S_{in}=K(S,D)/D+S.$$

In particular, if the equation $C_4(S)=0$ has n solutions S_i, $i=1,\ldots,n$, we put

$$\sigma_{i+2}=K(S_i,D)/D+S_i. \tag{32}$$

Note that we started with σ_3 because σ_1 and σ_2 are reserved for the transcritical bifurcations since they are less than σ_3 (see Table 5). Finally, using a procedure

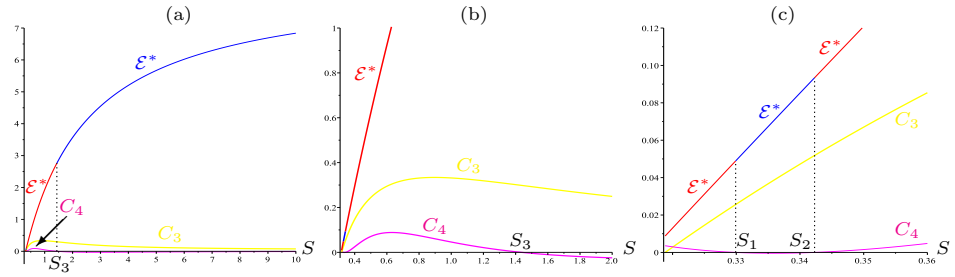

FIGURE 4. (a) Steady-state characteristics describing the local asymptotic behavior of the positive steady state $\mathcal{E}^*$ when $D = 0.25$. Magnification for (b) $S \leqslant 2$ and (c) $0.32 \leqslant S \leqslant 0.36$.

in D, we can determine the subset Υ_4 corresponding to Hopf bifurcation in the operating diagram of Fig. 6.

For the set of parameters in Table 7 corresponding to the operating diagram in Fig. 6, the numerical simulations show that the equation $C_4(S) = 0$ has three solutions S_i, $i = 1, 2, 3$ for $0 < D < D^* \simeq 0.2648$ (see Fig. 5). Using (32), we can deduce the corresponding three critical values σ_i, $i = 3, 4, 5$, which are provided in Table 5 and shown in Fig. 9. Moreover, these critical values correspond to the subset Υ_4 in Fig. 6. However, when $D^* < D < D_{\max} \simeq 1.595$, the equation $c_4(S) = 0$ has a unique solution S_1 that corresponds to the unique critical value σ_3.

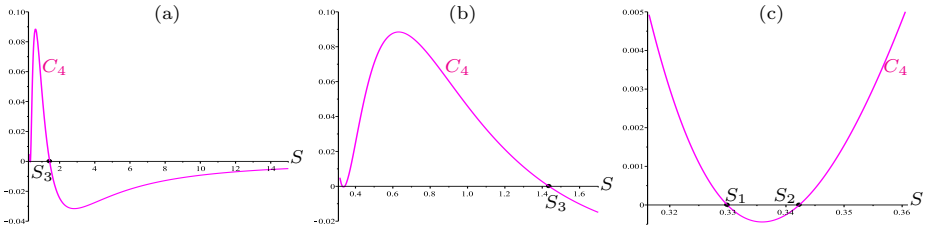

FIGURE 5. Case $D = 0.25 \leqslant D^* \simeq 0.2648$: (a) Change of sign of C_4 when $S_1 \simeq 0.3299$ (or equivalently $\sigma_3 \simeq 0.5255$), $S_2 \simeq 0.3423$ (or equivalently $\sigma_4 \simeq 0.7159$) and $S_3 \simeq 1.4365$ (or equivalently $\sigma_5 \simeq 12.4809$). (b) Magnification for $S \in [0.316, 1.7]$ and (c) magnification for $S \in [0.316, 0.361]$.

The following result determines the operating diagram for specific growth rates (31) and a set of parameters in Table 7.

Proposition 7. *For the biological parameter values provided in Table 7, the existence and the stability of the steady states of (1) in the four regions $\mathcal{J}_k$, $k = 1, \ldots, 4$ of the operating diagram are determined in Table 3.*

In the following, we used MATCONT [35] to determine the operating diagram presented in Fig. 7. In fact, MATCONT is a MATLAB software package for the numerical study of the continuation of steady states according to one parameter and the various bifurcations according to one or two parameters. It has many features and supports many functions, e.g. the continuation of branch points of steady states, limit cycles, homoclinic orbits, the detection of branch points, and Hopf bifurcation, etc. See [13] and the references therein for more details. Although the numerical operating diagram is identical to the theoretical one in Fig. 6, it must

TABLE 3. Existence and stability of steady states according to regions in the operating diagrams of Figs. 6 and 7. The letter S (resp. U) means stable (resp. unstable) steady state. Absence of letter means that the corresponding steady state does not exist.

Condition	Region	Color	$\mathcal{E}_0$	$\mathcal{E}_1$	$\mathcal{E}^*$
$S_{in} < \lambda_1(D)$	$\mathcal{J}_1$	Cyan	S		
$\lambda_1(D) < S_{in} < \varphi(D)$	$\mathcal{J}_2$	Pink	U	S	
$\varphi(D) < S_{in}$ and $c_4(S_{in}, D) > 0$	$\mathcal{J}_3$	Grey	U	U	S
$\varphi(D) < S_{in}$ and $c_4(S_{in}, D) < 0$	$\mathcal{J}_4$	Yellow	U	U	U

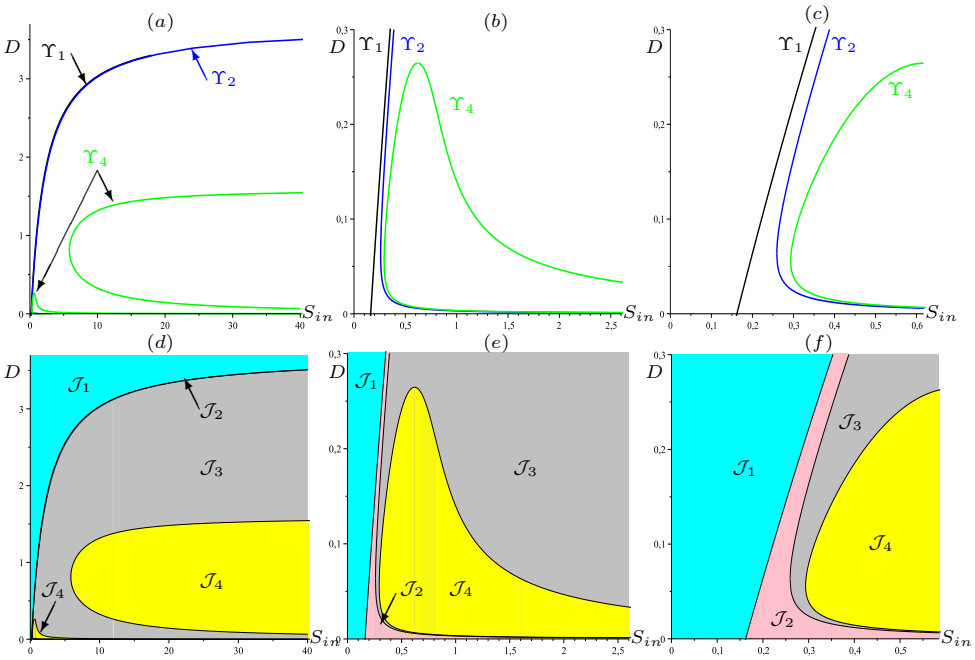

FIGURE 6. Operating diagram of (1) in MAPLE. (b)-(e) Magnification when $(S_{in}, D) \in [0, 2.6] \times [0, 0.3]$. (c)-(f) Magnification when $(S_{in}, D) \in [0, 0.6] \times [0, 0.3]$.

be stressed that they were obtained by completely different methods. The diagram in Fig. 6 is obtained by using our theoretical results and drawing the Υ_i subsets, defined in Table 2, that separate the different regions of the operating diagram, whereas the diagram in Fig. 7 is obtained numerically using MATCONT.

Proposition 8 records the nature of all bifurcations occurring as (S_{in}, D) crosses curves in the set Υ and steady states coalesce or change stability.

Proposition 8. *The bifurcation analysis of the steady states of (1) by crossing the curves of Υ according to the operating parameters S_{in} and D is summarized in Table 4.*

Figs. 8(a)-(c) illustrate how the coexistence region $\mathcal{J}_4$ around a stable limit cycle is reduced and eventually disappears as the mortality rates a_1 and a_2 defined in the introduction of system (1) tend to zero. They support our result in [36] that the process cannot admit a limit cycle if there is no mortality.

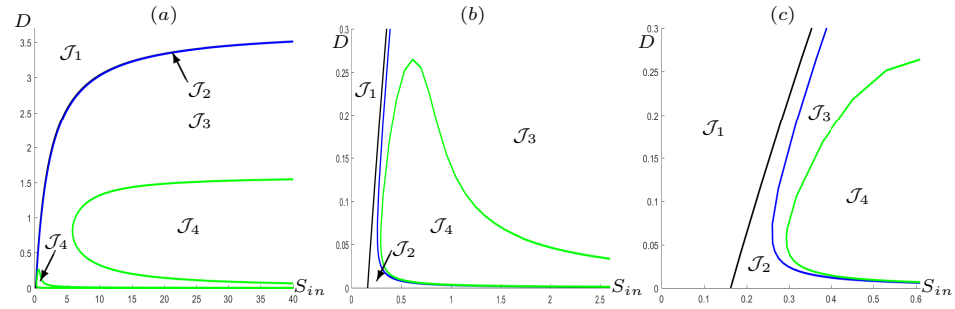

FIGURE 7. Operating diagram of (1) in MATCONT. (b) Magnification when $(S_{in}, D) \in [0, 2.6] \times [0, 0.3]$. (c) Magnification when $(S_{in}, D) \in [0, 0.6] \times [0, 0.3]$.

TABLE 4. Nature of bifurcations of the steady states of (1) by crossing to the surfaces of Υ. The letter TB (resp. SHB) means a transcritical bifurcation (resp. Supercritical Hopf bifurcation).

Subset	Transition	Bifurcation
Υ_1	$\mathcal{J}_1$ to $\mathcal{J}_2$	TB: $\mathcal{E}_0 = \mathcal{E}_1$
Υ_2	$\mathcal{J}_2$ to $\mathcal{J}_3$	TB: $\mathcal{E}_1 = \mathcal{E}^*$
Υ_4	$\mathcal{J}_3$ to $\mathcal{J}_4$	SHB: $\mathcal{E}^*$

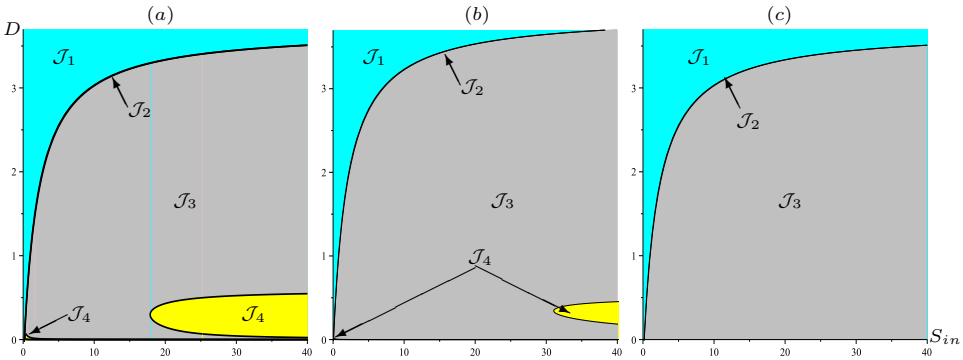

FIGURE 8. Operating diagram of (1) showing the disappearance of the region $\mathcal{J}_4$ when a_1 and a_2 diminish.

4. **A one-parameter bifurcation diagram and Hopf bifurcations.** In this section, we employ the package Scilab to make a representation of the evolution of the bifurcations in the system using the input substrate concentration S_{in} as the bifurcation parameter, while the dilution rate D is held fixed. Scilab is also used to prepare snapshots showing interesting trajectories for non-bifurcation values of the parameters before and after Hopf bifurcations. All other parameters of system (1) are fixed (see Table 7). In a similar way, we can study the one-parameter bifurcation diagram where the dilution rate D is the bifurcation parameter. The following result determines the one-parameter bifurcation diagram according to S_{in} from the operating diagram of Fig. 6 (or equivalently of Fig. 7) when the dilution rate $D = 0.25$.

Proposition 9. *Assume that the biological parameters in (1) are given as in Table 7 using the specific growth rates (31) with* $D = 0.25$. *The existence and stability*

of steady states of (1) according to S_{in} are given in Table 6 where the bifurcation values σ_i, $i = 1, \ldots, 5$ and the corresponding nature of the bifurcations are defined in Table 5.

TABLE 5. Definitions of the critical values σ_i, $i = 1, \ldots, 5$ of S_{in} and the corresponding nature of bifurcations when $D = 0.25$.

Definition	Value	Bifurcation
$\sigma_1 = \lambda_1(D)$	0.31884	TB
$\sigma_2 = \varphi(D)$	0.35394	TB
σ_3 is the first solution of equation $c_4(S_{in}) = 0$	0.52555	SHB
σ_4 is the second solution of equation $c_4(S_{in}) = 0$	0.71593	SHB
σ_5 is the third solution of equation $c_4(S_{in}) = 0$	12.4809	SHB

TABLE 6. Existence and stability of steady states according to S_{in}.

Interval of S_{in}	$\mathcal{E}_0$	$\mathcal{E}_1$	$\mathcal{E}^*$
$(0, \sigma_1)$	S		
(σ_1, σ_2)	U	S	
(σ_2, σ_3)	U	U	S
(σ_3, σ_4)	U	U	U
(σ_4, σ_5)	U	U	S
$(\sigma_5, +\infty)$	U	U	U

Fig. 9 represents the one-parameter bifurcation diagram of system (1) where the ω-limit set is projected to the coordinate S depending on the control parameter S_{in}. Indeed, in Fig. 9(a), we observe more clearly the transcritical bifurcations occurring at σ_1 and σ_2, and the appearance of a stable limit cycle via a supercritical Hopf bifurcation at σ_3 and its disappearance via a second supercritical Hopf bifurcation at σ_4. Increasing S_{in} further, another stable limit cycle emerges through a supercritical Hopf bifurcation at σ_5 as illustrated in Fig. 9(b). Then, the oscillations are sustained for all $S_{in} > \sigma_5$.

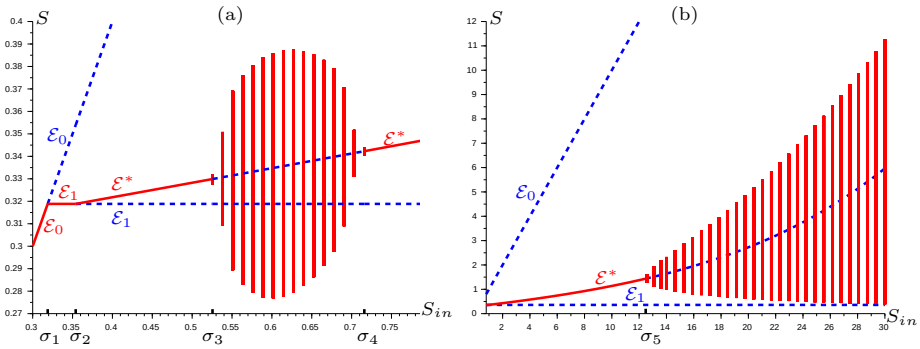

FIGURE 9. Scilab simulation showing projections of the ω-limit set in variable S when $D = 0.25$: (a) emergence and the disappearance of limit cycle at σ_3 and σ_4 for $S_{in} \in [0.3, 0.8]$; (b) emergence of limit cycle at σ_5 for $S_{in} \in [0.8, 30]$.

To understand and analyze the change of local stability occurring through the positive steady state $\mathcal{E}^*$ as S_{in} varies, we determine numerically the eigenvalues of the Jacobian matrix J at $\mathcal{E}^*$ by computing the roots of the characteristic polynomial (21). All biological parameters are fixed together with the dilution rate D. Indeed, this characteristic polynomial has one negative eigenvalue and one pair of complex-conjugate eigenvalues

$$\lambda_{\pm} = \mu(S_{in}) \pm i\nu(S_{in}). \tag{33}$$

As shown in Fig. 10, as the operating parameter S_{in} increases beyond σ_2, the value at which the positive steady state appears, the real part of the conjugate pair of eigenvalues is negative. The real parts transition to positive when S_{in} reaches $\sigma_4 \simeq 0.53$ and back to negative when S_{in} reaches $\sigma_4 \simeq 0.72$. In this particular example, the last transition from negative real part to positive real part occurs when S_{in} reaches $\sigma_5 \simeq 12.48$. In addition, numerically, we check the following inequality

$$\frac{d\mu}{dS_{in}}(\sigma_i) \neq 0, \quad i = 3, 4, 5. \tag{34}$$

This is consistent with Fig. 9, showing that, as S_{in} increases and crosses σ_i, $i = 3, 4, 5$, the positive steady state $\mathcal{E}^*$ changes its stability through three supercritical Hopf bifurcations with the occurrence or disappearance of a stable limit cycle that we illustrate in Figs. 12 and 13.

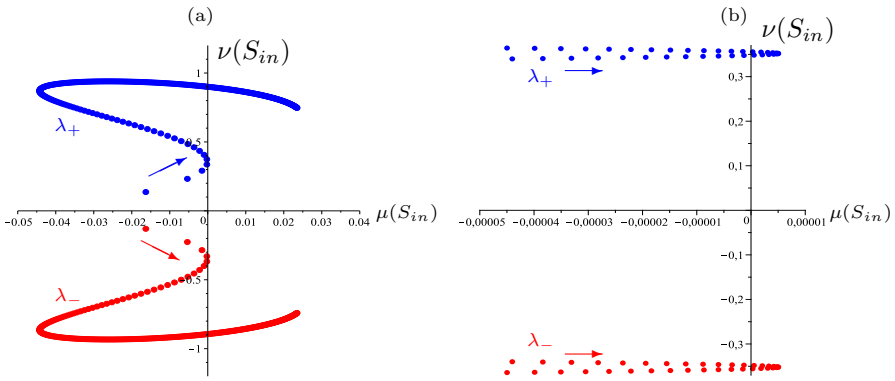

FIGURE 10. (a) Variation of the pair of complex-conjugate eigenvalues (33) as S_{in} increases from 0 to 40 when $D = 0.25$. (b) Magnification on $\lambda_{\pm}$ for $S_{in} \in [0.4, 0.8]$.

To validate the previous results, we illustrate in the following the three-dimensional phase plot and the trajectories over time in some interesting cases.

- For $S_{in} \in (\sigma_2, \sigma_3)$, the numerical simulations done in the three-dimensional phase space (S, x_1, x_2) for various positive initial conditions permit to conjecture the global convergence towards $\mathcal{E}^*$ (see Fig. 11).
- For $S_{in} \in (\sigma_3, \sigma_4)$, the numerical simulations done for various positive initial conditions permit to conjecture the global asymptotic stability of a stable limit cycle (see Fig. 12).
- For $S_{in} > \sigma_5$, Fig. 13 shows from a neighborhood of $\mathcal{E}^*$ of size order $\epsilon = 10^{-3}$ that the system exhibits sustained oscillations of all quantities, suggesting the system evolves toward a stable limit cycle.

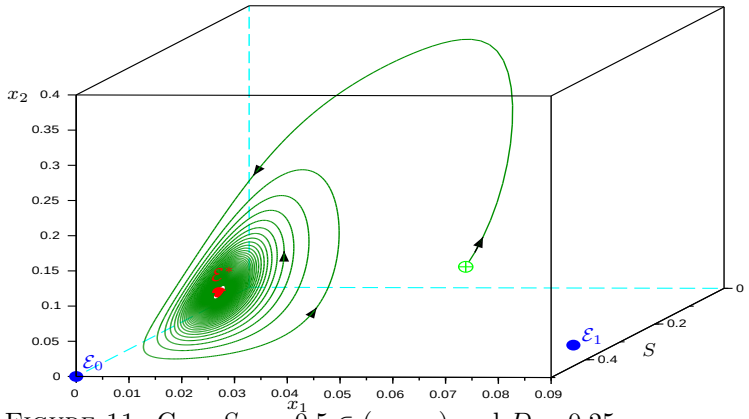

FIGURE 11. Case $S_{in} = 0.5 \in (\sigma_2, \sigma_3)$ and $D = 0.25$: convergence to $\mathcal{E}^*$.

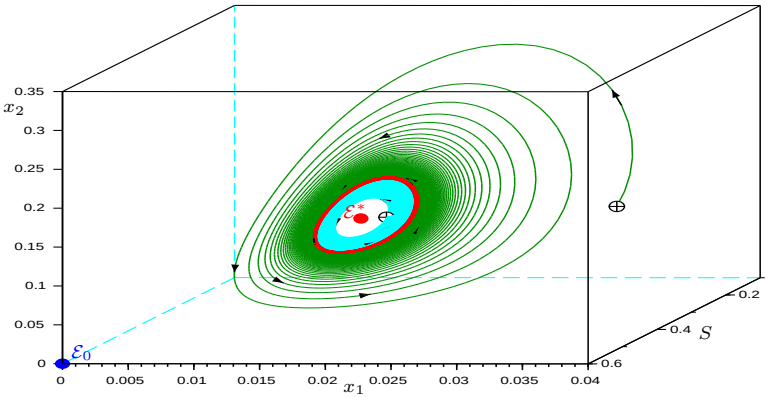

FIGURE 12. Case $S_{in} = 0.6 \in (\sigma_3, \sigma_4)$ and $D = 0.25$: convergence towards a stable limit cycle (in red).

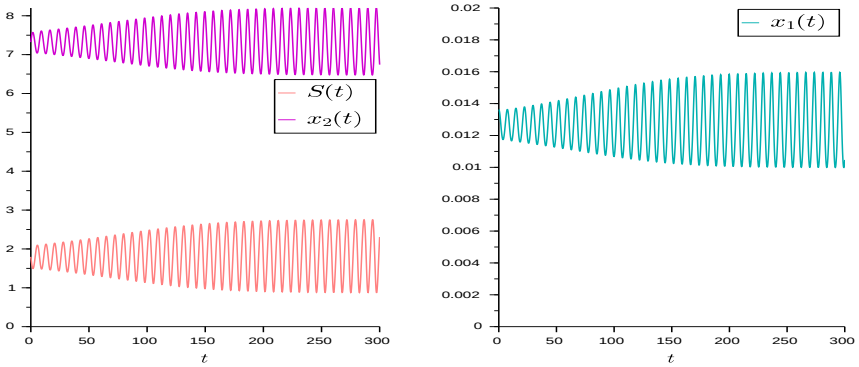

FIGURE 13. Case $S_{in} = 15 > \sigma_5$ and $D = 0.25$: convergence to a stable limit cycle showing the sustained oscillations.

5. **Conclusion.** In this paper, we have analysed an interspecific density dependent model of a predator-prey relationship between two microbial species in a chemostat, taking into consideration mortality with distinct removal rates. Under general growth functions, we give a complete analysis of system (1) by determining theoretically the operating diagram. The illustration of this diagram as well as the one-parameter bifurcation diagram and the Hopf bifurcations are obtained by specializing these functions.

Using the nullcline method [17, 36], the necessary and sufficient conditions of existence of all steady states of (1) are determined according to the parameter control. Indeed, this method provides a geometric description of the existence of the boundary steady states which are unique, and the multiplicity of the positive steady states. For the local stability of the positive steady state, we have used the Routh–Hurwitz criterion (23) since we cannot determine explicitly the eigenvalues of the Jacobian matrix at this point, in contrast to the boundary steady states, the stability conditions are determined explicitly. We show that the positive steady state can destabilize with the emergence of a stable limit cycle via a supercritical Hopf bifurcation.

Using the necessary and sufficient conditions of existence and stability of all steady states, the operating diagrams are analyzed analytically to determine the behavior of the system according to the concentration of substrate in the feed bottle S_{in} and the dilution rate D. These conditions are plotted in MAPLE using specific growth functions given by (31). Then, these theoretical results on the operating diagram are validated numerically using MATCONT.

In fact, the process exhibits an even richer set of possible behaviors illustrated in the operating diagram: either the washout ($\mathcal{J}_1$) or the exclusion of the predator ($\mathcal{J}_2$) or the coexistence of the predator-prey species around a positive steady state ($\mathcal{J}_3$) or a stable limit cycles ($\mathcal{J}_4$). The one-parameter bifurcation diagram is determined according to the input substrate concentration S_{in} as the bifurcating parameter. It shows the transcritical bifurcation as well as the three supercritical Hopf bifurcations with the appearance and the disappearance of the stable periodic orbits. The numerical simulations illustrate the three-dimensional phase space showing the coexistence around a coexistence steady state or a stable limit cycle, while the time course shows the sustained oscillations.

The comparison of our results with those in the existing literature [14, 36] proves that the addition of mortality terms of the species in the interspecific density-dependent model (1) with a predator-prey relationship can destabilize the positive steady states. However, the addition of mortality does not change the global behavior of the process where there can be either washout of the two species or exclusion of the predator, or coexistence of the two species around a steady state or a stable limit cycle.

Appendix A. **Parameter values used for numerical simulations.** All the values of the parameters used in the numerical simulations are provided in Table 7.

Appendix B. **Auxiliary functions used in the paper.** For the convenience of the reader, we summarize in Table 8 all the auxiliary functions that were used in this paper.

TABLE 7. Parameter values used for model (1) when the growth rates f_1 and f_2 are given by (31).

Parameter	m_1	K_1	L_1	m_2	K_2	L_2	α_1	α_2	a_1	a_2
Fig. 2(c)	2.75	2	1.2	2.95	1.8	1.5	10^{-3}	0.1	0.95	0.7
Figs. 1,2(a,b),6,7,9–13	4	2	3	8	0.1	0.2	1	1	0.3	0.2
Fig. 8(a)									0.3	0.05
Fig. 8(b)									0.1	0.05
Fig. 8(c)									0	0

TABLE 8. Break-even concentration, notations and auxiliary functions.

$\lambda_1(D)$	$S = \lambda_1(D)$ is the solution of equation $f_1(S,0) = \alpha_1 D + a_1$ It is defined for $D < (f_1(+\infty,0) - a_1)/\alpha_1$, see (4)
$\tilde{x}_1$	$\tilde{x}_1 = \frac{D}{D_1}(S_{in} - \lambda_1(D))$, see (5)
$\widetilde{f}_1(x_1,x_2)$	$\widetilde{f}_1(x_1,x_2) = f_1(S_{in} - \frac{D_1}{D}x_1 - \frac{D_2}{D}x_2, x_2) - D_1$, see (11)
$\widetilde{f}_2(x_1,x_2)$	$\widetilde{f}_2(x_1,x_2) = f_2(S_{in} - \frac{D_1}{D}x_1 - \frac{D_2}{D}x_2, x_1) - D_2$, see (11)
$F_1(x_1)$	$x_2 = F_1(x_1)$ is the unique solution of equation $\widetilde{f}_1(x_1,x_2) = 0$ It is defined for $0 \le x_1 \le \tilde{x}_1$, see Lemma 1
$F_2(x_1)$	$x_2 = F_2(x_1)$ is the unique solution of equation $\widetilde{f}_2(x_1,x_2) = 0$ It is defined for $x_1^1 \le x_1 \le x_1^2$, where x_1^1 and x_1^2 are the solutions of equation $\widetilde{f}_2(x_1,0) = 0$, see Lemma 3
(x_1^*, x_2^*)	(x_1^*, x_2^*) is a solution of $x_2 = F_1(x_1) = F_2(x_1)$, see Prop. 3
$X_1(S,D)$	$x_1 = X_1(S,D)$ is the solution of equation $f_2(S,x_1) = \alpha_2 D + a_2$ It is defined for $S > \lambda_2'(D)$, where $\lambda_2'(D)$ is the unique solution, if it exists, of equation $f_2(S,+\infty) = \alpha_2 D + a_2$, see (26)
$X_2(S,D)$	$x_2 = X_2(S,D)$ is the solution of equation $f_1(S,x_2) = \alpha_1 D + a_1$ It is defined for $\lambda_1(D) \le S < \lambda_1'(D)$, where $\lambda_1'(D)$ is the unique solution, if it exists, of equation $f_1(S,+\infty) = \alpha_1 D + a_1$, see (25)
$\varphi(D)$	$\varphi(D) = \lambda_1(D) + \frac{D_1}{D}X_1(\lambda_1(D), D)$, see (27)
$K(S,D)$	$K(S,D) = D_1 X_1(S,D) + D_2 X_2(S,D)$, see (30)

Acknowledgments. The first author thanks the Tunisian Ministry of Higher Education, Scientific Research and Technology for financial support and INRAE for hosting her in Montpellier during the preparation of this work. The authors are grateful to two anonymous reviewers for their insightful comments and suggestions that greatly improved this manuscript.

REFERENCES

[1] N. Abdellatif, R. Fekih-Salem and T. Sari, Competition for a single resource and coexistence of several species in the chemostat, *Math. Biosci. Eng.*, *13* (2016), 631–652.
[2] M. Ballyk, R. Staffeldt and I. Jawarneh, A nutrient-prey-predator model: Stability and bifurcations, *Discrete & Continuous Dyn. Syst. - S*, *13* (2020), 2975–3004.
[3] B. Bar and T. Sari, The operating diagram for a model of competition in a chemostat with an external lethal inhibitor, *Discrete & Continuous Dyn. Syst. - B*, **25** (2020), 2093–2120.
[4] B. Benyahia, T. Sari, B. Cherki and J. Harmand, Bifurcation and stability analysis of a two step model for monitoring anaerobic digestion processes, *J. Proc. Control*, **22** (2012), 1008–1019.

[5] O. Bernard, Z. Hadj-Sadok, D. Dochain, A. Genovesi and J-P. Steyer, Dynamical model development and parameter identification for an anaerobic wastewater treatment process, *Biotechnol. Bioeng.*, **75** (2001), 424–438.
[6] M.P. Boer, B.W. Kooi and S.A.L.M. Kooijman, Food chain dynamics in the chemostat, *Math. Biosci.*, **150** (1998), 43–62.
[7] F. Borsali and K. Yadi, Contribution to the study of the effect of the interspecificity on a two nutrients competition model, *Int. J. Biomath.*, **8** (2015), 1550008, 17 pp.
[8] M. Dali-Youcef, A. Rapaport, and T. Sari, Study of performance criteria of serial configuration of two chemostats, *Math. Biosci. Eng.*, **17** (2020), 6278–6309.
[9] Y. Daoud, N. Abdellatif, T. Sari, and J. Harmand, Steady state analysis of a syntrophic model: The effect of a new input substrate concentration, *Math. Model. Nat. Phenom.*, **13** (2018), 1–22.
[10] P. De Leenheer, D. Angeli and E.D. Sontag, Crowding effects promote coexistence in the chemostat, *J. Math. Anal. Appl.*, **319** (2006), 48–60.
[11] M. Dellal and B. Bar, Global analysis of a model of competition in the chemostat with internal inhibitor, *Discrete & Continuous Dyn. Syst. - B*, **26** (2021), 1129–1148.
[12] M. Dellal, M. Lakrib and T. Sari, The operating diagram of a model of two competitors in a chemostat with an external inhibitor, *Math. Biosci.*, **302** (2018), 27–45.
[13] A. Dhooge, W. Govaerts, Yu. A. Kuznetsov, H.G.E. Meijer and B. Sautois, New features of the software MatCont for bifurcation analysis of dynamical systems, *Mathematical and Computer Modelling of Dynamical Systems*, **14** (2008), 147–175.
[14] M. El-Hajji, How can inter-specific interferences explain coexistence or confirm the competitive exclusion principle in a chemostat?, *Int. J. Biomath.*, **11** (2018), 1850111, 20 pp.
[15] M. El-Hajji, F. Mazenc and J. Harmand, A mathematical study of a syntrophic relationship of a model of anaerobic digestion process, *Math. Biosci. Eng.*, **7** (2010), 641–656.
[16] R. Fekih-Salem, J. Harmand, C. Lobry, A. Rapaport and T. Sari, Extensions of the chemostat model with flocculation, *J. Math. Anal. Appl.*, **397** (2013), 292–306.
[17] R. Fekih-Salem, C. Lobry and T. Sari, A density-dependent model of competition for one resource in the chemostat, *Math. Biosc.*, **268** (2017), 104–122.
[18] R. Fekih-Salem, A. Rapaport and T. Sari, Emergence of coexistence and limit cycles in the chemostat model with flocculation for a general class of functional responses, *Appl. Math. Modell.*, **40** (2016), 7656–7677.
[19] R. Fekih-Salem and T. Sari, Properties of the chemostat model with aggregated biomass and distinct removal rates, *SIAM J. Appl. Dyn. Syst. (SIADS)*, **18** (2019), 481–509.
[20] R. Fekih-Salem and T. Sari, Operating diagram of a flocculation model in the chemostat, *ARIMA J.*, **31** (2020), 45–58.
[21] B. Haegeman and A. Rapaport, How flocculation can explain coexistence in the chemostat, *J. Biol. Dyn.*, **2** (2008), 1–13.
[22] M. Hanaki, J. Harmand, Z. Mghazli, A. Rapaport, T. Sari, and P. Ugalde, Mathematical Study of a Two-Stage Anaerobic Model When the Hydrolysis Is the Limiting Step, *Processes*, **9** (2021).
[23] S.R. Hansen and S.P. Hubbell, Single-nutrient microbial competition: Qualitative agreement between experimental and theoretically forecast outcomes, *Science*, (1980), 1491–1493.
[24] J. Harmand, C. Lobry, A. Rapaport and T. Sari, The Chemostat: Mathematical Theory of Microorganism Cultures, vol. 1, *Chemical Eng. Ser., Chemostat Bioprocesses Set, Wiley, New York.*, (2017).
[25] J. Harmand, A. Rapaport, D. Dochain and C. Lobry, Microbial ecology and bioprocess control: Opportunities and challenges, *Journal of Process Control*, **18** (2008), 865–875.
[26] S.-B. Hsu, C.A. Klausmeier and C.-J. Lin, Analysis of a model of two parallel food chains, *Discrete & Continuous Dyn. Syst. - B*, **12** (2009), 337–359.
[27] Z. Khedim, B. Benyahia, B. Cherki, T. Sari and J. Harmand, Effect of control parameters on biogas production during the anaerobic digestion of protein-rich substrates, *Appl. Math. Model.*, **61** (2018), 351–376.
[28] B.W. Kooi and M.P. Boer, Chaotic behaviour of a predator-prey system in the chemostat, *Dyn. Contin. Discrete Impuls. Syst. Ser. B Appl. Algorithms*, **10** (2003), 259–272.
[29] B. Li and Y. Kuang, Simple food chain in a chemostat with distinct removal rates, *J. Math. Anal. Appl.*, **242** (2000), 75–92.
[30] C. Lobry and J. Harmand, A new hypothesis to explain the coexistence of n species in the presence of a single resource, *C. R. Biol.*, **329** (2006), 40–46.

[31] C. Lobry and F. Mazenc, Effect on persistence of intra-specific competition in competition models, *Electron. J. Diff. Equ.*, **125** (2007), 1–10.
[32] C. Lobry, F. Mazenc and A. Rapaport, Persistence in ecological models of competition for a single resource, *C. R. Acad. Sci. Paris, Ser. I*, **340** (2005), 199–204.
[33] C. Lobry, A. Rapaport and F. Mazenc, Sur un modèle densité-dépendant de compétition pour une ressource, *C. R. Biol.*, **329** (2006), 63–70.
[34] MAPLE [Software], Version 13.0, *Maplesoft*, a division of Waterloo Maple Inc., Waterloo, Ontario (2009).
[35] MATCONT [Software]. *https://sourceforge.net/projects/matcont/?source=directory.*
[36] T. Mtar, R. Fekih-Salem and T. Sari, Interspecific density-dependent model of predator-prey relationship in the chemostat, *Int. J. Biomath.*, **14** (2021), 2050086, 22 pp.
[37] T. Mtar, R. Fekih-Salem and T. Sari, Effect of the mortality on a density-dependent model with a predator-prey relationship, *CARI'2020, Proceedings of the 15th African Conference on Research in Computer Science and Applied Mathematics*, *hal-02912854v2*, (2020).
[38] S. Nouaoura, R. Fekih-Salem, N. Abdellatif and T. Sari, Mathematical analysis of a three-tiered food-web in the chemostat, *Discrete & Contin. Dyn. Syst. Ser. B*, **26** (2021), 5601–5625.
[39] S. Nouaoura, N. Abdellatif, R. Fekih-Salem and T. Sari, Mathematical analysis of a three-tiered model of anaerobic digestion, *SIAM - Journal on Applied Mathematics (SIAP)*, **81** (2021), 1264–1286.
[40] S. Nouaoura, R. Fekih-Salem, N. Abdellatif and T. Sari, Operating diagrams for a three-tiered microbial food web in the chemostat, *Preprint HAL* (2021).
[41] A. Rapaport and M. Veruete, A new proof of the competitive exclusion principle in the chemostat, *Discrete & Continuous Dyn. Syst. - B*, **24** (2019), 3755–3764.
[42] T. Sari and B. Benyahia, The operating diagram for a two-step anaerobic digestion model, *Nonlinear Dynam.*, **105** (2021), 2711–2737.
[43] T. Sari and J. Harmand, A model of a syntrophic relationship between two microbial species in a chemostat including maintenance, *Math. Biosci.*, **275** (2016), 1–9.
[44] T. Sari and M.J. Wade, Generalised approach to modelling a three-tiered microbial food-web, *Math. Biosci.*, **291** (2017), 21–37.
[45] M. Sbarciog, M. Loccufier and E. Noldus, Determination of appropriate operating strategies for anaerobic digestion systems, *Biochem. Eng. J.*, **51** (2010), 180–188.
[46] SCILAB [Software], version 6.0.1, *Scilab* Enterprises SAS (2018).
[47] S. Shen, G.C. Premier, A. Guwy, and R. Dinsdale, Bifurcation and stability analysis of an anaerobic digestion model, *Nonlinear Dynam.*, **48** (2007), 391–408.
[48] S. Sobieszek and M.J. Wade and G.S.K. Wolkowicz, Rich dynamics of a three-tiered anaerobic food-web in a chemostat with multiple substrate inflow, *Math. Biosci. Eng.*, **17** (2020), 7045–7073.
[49] H.L. Smith and P. Waltman, The Theory of the Chemostat, Dynamics of Microbial Competition, *Cambridge University Press*, (1995).
[50] G.A.K. Van Voorn, B.W. Kooi and M.P. Boer, Ecological consequences of global bifurcations in some food chain models, *Math. Biosci.*, **226** (2010), 120–133.
[51] D.V. Vayenas and S. Pavlou, Chaotic dynamics of a food web in a chemostat, *Math. Biosci.*, **162** (1999), 69–84.
[52] M.J. Wade and R.W. Pattinson and N.G. Parker and J. Dolfing, Emergent behaviour in a chlorophenol-mineralising three-tiered microbial 'food web', *J. Theor. Biol.*, **389** (2016), 171–186.
[53] M.J. Wade and J. Oakley and S. Harbisher and N.G. Parker and J. Dolfing, MI-Sim: A MATLAB package for the numerical analysis of microbial ecological interactions, *PLoS ONE*, **12**(3) (2017), e0173249.
[54] M. Weedermann, G.S.K. Wolkowicz and J. Sasara, Optimal biogas production in a model for anaerobic digestion, *Nonlinear Dyn.*, **81** (2015), 1097–1112.
[55] G.S.K. Wolkowicz, Successful invasion of a food web in a chemostat, *Math. Biosci.*, **93** (1989), 249–268.
[56] A. Xu, J. Dolfing, T.P. Curtis, G. Montague and E. Martin, Maintenance affects the stability of a two-tiered microbial 'food chain'?, *J. Theor. Biol.*, **276** (2011), 35–41.

E-mail address: tahani.mtar@enit.utm.tn
E-mail address: radhouane.fekih-salem@enit.utm.tn
E-mail address: tewfik.sari@inrae.fr